Journal of Thermal Analysis and Calorimetry, Vol. 69 (2002) 9–21

^{18}O-ISOTOPE EXCHANGE BEHAVIOUR AND OXIDATION ACTIVITY OF $La_{1-x}Sr_xMnO_{3+\delta}$

I. K. Murwani, S. Scheurell, M. Feist, and E. Kemnitz

Institute of Chemistry, Humboldt University, Hessische Str. 1-2, D-10115 Berlin, Germany

Abstract

Different preparation routes derived both from the usual high-temperature solid state synthesis and the sol–gel process were applied for the synthesis of crystalline $La_{1-x}Sr_xMnO_{3+\delta}$ phases with $0 \leq x \leq 0.2$. They were investigated by means of temperature programmed isotope exchange (TPIE) under various conditions. The ^{18}O isotope exchange experiments yielded information on the dependence of the oxygen mobility on temperature and the Mn^{4+}/Mn^{3+} ratio. Both are related to the defect structure of the solid. TPIE was applied for studying the interaction between $^{18}O_2$ and CH_4 under static conditions and was compared with results obtained from catalytic investigations, i.e. the behaviour of $La_{1-x}Sr_xMnO_{3+\delta}$ ($0 \leq x \leq 0.2$) in both CO and CH_4 oxidation with normal oxygen $^{16}O_2$ under steady flow conditions.

Keywords: catalytic activity, CO oxidation, methane oxidation, ^{18}O isotope exchange, ternary manganites

Introduction

The wide variety of dynamic thermal analysis (TA) methods comprises not only the conventional simultaneous methods such as TG-DTA and the modern simultaneously coupled methods such as TG-FTIR or TG-DTA-MS together with PulseTA® [1, 2]. The temperature programmed isotope exchange (TPIE) also represents an interesting variation of dynamic thermal analysis as it allows the following of the change of a sample property (e.g. the oxygen liberation of a solid) with an imposed temperature program. TPIE revealed to be especially promising for the investigation of the oxygen mobility in/onto solid oxide systems since the easy availability of the isotope ^{18}O allows for the investigation of how a gas atmosphere containing ^{18}O interacts with a solid containing the normal isotope ^{16}O. This method has been succesfully applied in the investigation of bulk and/or surface diffusion of metal oxides [3], high-temperature super conductors [4], ternary manganites [5] and others.

This work continues the investigations in [5] where manganites with perovskite ($LaMnO_3$ and $La_{0.7}Sr_{0.3}MnO_3$) and perovskite-like structures ($SrMnO_3$) were studied with respect to their catalytic activity in oxidation reactions. The substances were obtained by high-temperature solid state synthesis; our aim was now to study the influence of various synthesis conditions on the oxygen exchange properties and the catalytic activity as well.

1418–2874/2002/ $ 5.00

Akadémiai Kiadó, Budapest
Kluwer Academic Publishers, Dordrecht

The possible application of perovskite type oxides in catalysis was firstly reported in 1952 for the CO oxidation, whereby the potential of these oxides as automatic exhaust oxidation catalysts had already been mentioned [6, 7]. Since then, numerous investigations have been directed to the catalytic activity of perovskites in different reactions, such as the reduction of NO_x with different reductants like carbon monoxide [6] or in hydrogenation reactions (e.g. propylene) [8]. Perovskites like $LaMnO_3$ as well as La_2MnO_4 have been shown to catalyze the oxidation of CO and hydrocarbons [9].

The ideal perovskite structure, ABO_3 can be envisaged to consist of closed hexagonally packed sheets of AO_3 in which the big A cation is surrounded by six oxygen ions. In cubic perovskites, these AO_3 sheets are stacked in the sequence abcabc and all octahedral holes are occupied by the smaller B cation. These B cations, which are usually transition metals, are the catalytically active centers [10]. A cations may be alkaline earth elements such as calcium, strontium, barium or other basic metals like bismuth or lead. Rare earth ions occupying the A-site increase the thermal stability of the material [11].

Perovskites are frequently non-stoichiometric which is expressed by the formula $ABO_{3+\delta}$ where δ is usually between +0.1 and –0.5. Cationic substitution in A or B sublattices by lower valency ions can impose various consequences which are especially interesting if B can adopt different oxidation states, e.g. B^{III}/B^{IV}. If A is substituted and the oxygen stoichiometry remains unchanged, a corresponding fraction of B^{IV} will be formed. The same result is yielded when B^{III} is substituted. If, however, no B^{IV} formation occurs, oxygen is released thus producing oxygen vacancies in the remaining solid. The thermal stability of the perovskite structure makes these systems ideally suitable for studies on the correlation between catalytic activity and the type and density of defects.

Experimental

Synthesis procedures

Besides the usual high temperature solid state synthesis, which was applied for comparison as well, the $La_{1-x}Sr_xMnO_{3+\delta}$ samples were prepared by variations of the sol–gel process combined with pyrolysis treatments. The polyvinyl alcohol (PVA) method, the nitrate and the citric acid methods were applied for x=0, 0.1, 0.2. Stoichiometric amounts of analytical grade $La(NO_3)_3 \cdot 6H_2O$, $Sr(NO_3)_2$ and $Mn(NO_3)_2 \cdot 4H_2O$ were dissolved in distilled water. La and Mn solutions were mixed with 20 mL 15 mass% PVA solution. The resulting solution was mixed with a magnetic stirrer at ca. 100°C. A viscous gel was obtained after 2–3 h mixing. The gel was dried at 110°C for 12 h yielding a fairly porous dry gel. Several samples were treated by the pyrolysis method. The gel was poured out onto a thin polyethylene foil and was left until drying. The dry gel was separated from the plastic foil, then burned, so that a fine porous black powder was obtained. The product was calcined at 500–600°C for 24 h in flowing oxygen (20 mL min^{-1}). The nitrate method consists of mixing calculated amounts of the La^{3+} and Mn^{2+} nitrates followed by a slow heating up to 900°C and subsequent grinding. In the citrate method, the corresponding nitrate salts were dissolved in small amounts of water and citrate acid solution was added in an appropri-

ate amount to replace all the nitrate groups by citrate groups. The nitrate salt solutions were mixed and continuously stirred using a magnetic stirrer. Then, the mixed solution was poured into a dish and heated at 135°C under constant stirring to transform it into a xerogel. When ignited at any point of gelation in air at room temperature, the dried gel burned in a self-propagating combustion manner until all gels were completely burned out to form a loose powder. It was then followed by grinding and heating for 10 h at 600°C under atmospheric conditions, and, finally, calcined at 700°C for 12 h in flowing oxygen (20 mL min^{-1}).

Sample characterization

The samples were analyzed for C, H, N, S by usual elemental micro analysis techniques (CHNS 932, Leco Corp., St. Joseph. Mich., USA). The crystallinity was checked by a powder diffractometer XRD7 (Seiffert PM, Freiberg, Germany) using CuK_α-radiation, λ=1.54056 Å. Lattice constants were determined by the program TREOR [12]. The specific surface areas of the samples were measured by the BET standard method using N_2 adsorption at 77 K (ASAP 2000 system, Micromeritics).

According to [13], the determination of δ in $LaMnO_3$ was performed by thermogravimetric (TG) analysis in a Ar–H_2 flow and completed by iodometric determination of the ratio Mn(IV):Mn(III) [14].

TPIE measurements

The TPIE measurements were carried out in a quartz apparatus on line coupled to a quadrupole mass spectrometer QMG 421 I (Pfeiffer Vacuum GmbH). The experimental setup has been comprehensively described in [15]. Before starting the individual TPIE run, each sample has been subjected to a thermal pre-treatment. It consists of a 4 h tempering at 400°C in an air flow (p=150 Pa), in order to remove H_2O, CO_2, and other molecules from the surface of the oxide. After cooling down to 100°C, Ar, $^{16}O_2$ and $^{18}O_2$ were introduced into the reaction system where an initial total pressure of 150 Pa was adjusted with a pressure ratio of 1:2:2 (30 Pa Ar, 60 Pa $^{16}O_2$ and 60 Pa $^{18}O_2$). All measurements were performed in the temperature range of 100–700°C with a heating rate of 10 K min^{-1}. The variation of the gas phase composition during the heating run was followed by the QMS.

Evaluation of the TPIE data

During the interaction of a gas phase containing ^{18}O and a solid containing ^{16}O, oxygen uptake/release and three types of isotope exchange may occur consecutively and/or simultaneously. As these processes have been comprehensively elucidated elsewhere [16–18] and applied in previous papers [4, 5, 14], they only will be shortly summarized as follows.

a) Homomolecular isotope exchange.
b) Partial heteromolecular isotope exchange.
c) Complete heteromolecular isotope exchange.

Four different coefficients derived from the measured ion currents (IC) have been proposed [16–18]. They describe the partition of the oxygen isotopes between the gas phase and the solid. Their temperature dependence allows one to distinguish between the individual processes occuring simultaneously.

1) The coefficient *s* represents the oxygen partial pressure of the gas phase standardized by the oxygen partial pressure at the beginning of the measurement (*t*=0). The coefficient s changes only when uptake/release occurs, i.e. in-diffusion or out-diffusion.

$$s=\frac{p_i}{p_0}=\frac{\{[^{16}O_2]+[^{16}O^{18}O]+[^{18}O_2]\}_{t=i}}{\{[^{16}O_2]+[^{16}O^{18}O]+[^{18}O_2]\}_{t=0}} \quad (1)$$

2) The coefficient *c* expresses the proportion of ^{18}O relative to the total oxygen content in the gas phase. The value of *c* diminishes when, as a result of isotope exchange with the solid, the ^{18}O content in the gas phase decreases. Both the exchange and diffusion processes may be followed utilizing this coefficient.

$$c=\frac{\frac{[^{16}O^{18}O]}{2}+[^{18}O_2]}{[^{16}O_2]+[^{16}O^{18}O]+[^{18}O_2]} \quad (2)$$

3) Coefficient *y* describes the deviation of the actual partial pressure from the equilibrium partial pressure of $^{16}O^{18}O$ measured at *t*=i. For an initial partial pressure ratio $[^{16}O_2]:[^{18}O_2]=1:1$, the equilibrium partial pressure $[^{16}O^{18}O]_{eq}$ amounts to 0.5, thus *y*=0.

$$y=\left[\frac{[^{16}O^{18}O]}{[^{16}O_2]+[^{16}O^{18}O]+[^{18}O_2]}\right]_{eq}-\left[\frac{[^{16}O^{18}O]}{[^{16}O_2]+[^{16}O^{18}O]+[^{18}O_2]}\right]_{t=i}= \quad (3)$$

$$y=0.5-\left[\frac{[^{16}O^{18}O]}{[^{16}O_2]+[^{16}O^{18}O]+[^{18}O_2]}\right]_{t=i}$$

4) The coefficient *v* represents the fraction of ^{18}O in the gas phase that originates from the $^{16}O^{18}O$ molecules.

$$v=\left\{\frac{\frac{[^{16}O^{18}O]}{2}}{\frac{[^{16}O^{18}O]}{2}+[^{18}O_2]}\right\}_{t=i}\left\{\frac{\frac{[^{16}O^{18}O]}{2}+[^{18}O_2]}{\frac{[^{16}O^{18}O]}{2}}\right\}_{t=0} \quad (4)$$

Catalytic activity test

A packed-bed tubular quartz reactor (i.d. 4 mm) with a 5 mm o.d. thermowell has been utilized. The catalyst powder (ca. 600 mg) was pelleted, crushed, sieved to 0.5–1 mm grain size. The catalyst was placed in the middle of the cylinder, fixed by a small quartz holder and covered from both sides by quartz wool. The gas flows were controlled by MFCs. The catalytic activity has been tested as activity in CO and CH_4

oxidation. The catalyst was activated for 1 h in 20 mL min^{-1} flowing N_2 at 450°C. After cooling down to 25°C in N_2, the feeding of CO or CH_4 gas mixture was started. The CO oxidation was carried out by feeding the reactor with a flow of 6 CO and 6 mL min^{-1} O_2 (1:1), whereas for the CH_4 oxidation 2.4 of CH_4 and 9.6 mL min^{-1} of O_2 (1:4) have been applied. The gaseous product composition was analyzed on line by a gas chromatograph equipped with a TCD detector (Shimadzu GC-17A).

Results and discussion

Preparation routes

The following abbreviations (Table 1) are used to make recognizable the various types of sample preparation: SS – solid state synthesis at usual high temperatures; SG–CA–sol gel process with citric acid as reductant followed by drying and calcination; SGP–PVA–sol gel process with poly(vinyl alcohol) as reductant followed by pyrolysis of the thin film and calcination at given temperature.

Table 1 Sample characterization (abbreviations – see text)

Composition	Synthesis	Calcination temp./°C	C/%	S_{BET}/ $m^2\ g^{-1}$	XRD	Mn^{4+}/Mn^{3+}
$LaMnO_{3.10}$	SS	950	0.051	0.37	orth	0.25
$LaMnO_{3.13}$	SG–CA	700	0.108	16.27	rhom	0.35
$LaMnO_{3.15}$	SGP–PVA	600	0.359	16.56	rhom	0.40
$La_{0.9}Sr_{0.1}MnO_{3.01}$	SGP–PVA	600	0.437	24.94	cubic	0.14
$La_{0.8}Sr_{0.2}MnO_{3.05}$	SGP–PVA	600	0.468	21.12	rhom	0.42
$La_{0.9}Sr_{0.1}MnO_{3.07}$	SG–CA	700	0.302	17.26	cubic	0.32
$La_{0.8}Sr_{0.2}MnO_{3.16}$	SG–CA	700	0.354	18.07	hex	1.08

The nitrate–citrate gels which were obtained from the reaction of metal nitrates and citric acid exhibited a self-propagating combustion behavior. The combustion rate is associated with the molar ratio nitrates:citric acid. The most rapid combustion was observed for the gel with 1:1 ratio, and decreases with increasing amounts of citric acid [19]. The direct transformation of an amorphous gel during combustion into crystalline $La_{1-x}Sr_xMnO_{3+\delta}$ seems to be due to the higher degree of compositional homogeneity and the greater heat generated by the exothermic reaction of nitrates and citric acid. As the carbon chains in citrates are decomposed during combustion, adjacent atoms which are homogeneously distributed throughout the matrix can easily come into contact and form crystal lattices at a considerable rate. In addition, the crystallite size of the obtained powder depends on the molar ratio of nitrates to citric acid, which determines the combustion process and rate.

Sample characterization

The main results characterizing the investigated samples are summarized in Table 1. The values for the BET surface area exceed those reported for the conventionally prepared samples by ca one order of magnitude. The influence of the calcination temperatures on the BET area can be clearly noticed.

For instance, changing the synthesis type from SS to SG–CA for the same precursor yielded a sample surface of 16.27 $m^2 g^{-1}$, which causes a higher catalytic activity (see below). As for the present study structural properties were preferentially investigated, simple surface effects had to be avoided. Therefore, only samples without an amorphous background in X-ray diffractograms were selected for polythermal ^{18}O exchange experiments, and the sample mass was varied in such a way that the available surface area was approximately the same.

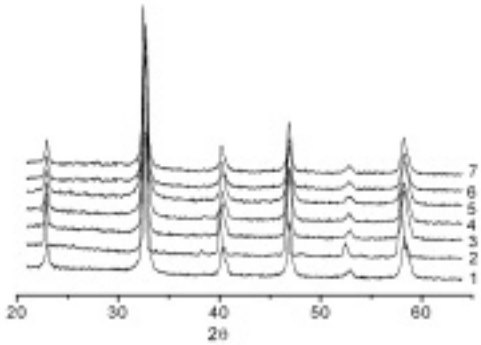

Fig. 1 XRD patterns of $La_{1-x}Sr_xMnO_{3+\delta}$ (x=0, 0.1, 0.2) for various preparation routes (for the abbreviations – see text): 1 – $LaMnO_{3.15}$ (SGP–PVA); 2 – $LaMnO_{3.10}$ (SS); 3 – $LaMnO_{3.13}$ (SG–CA); 4 – $La_{0.9}Sr_{0.1}MnO_{3.01}$ (SGP–PVA); 5 – $La_{0.8}Sr_{0.2}MnO_{3.05}$ (SGP–PVA); 6 – $La_{0.9}Sr_{0.1}MnO_{3.07}$ (SG–CA); 7 – $La_{0.8}Sr_{0.2}MnO_{3.16}$ (SG–CA)

The X-ray powder diffraction patterns of the $La_{1-x}Sr_xMnO_{3+\delta}$ (Fig. 1) proved that in all cases well-crystallized, single phase perovskites were formed. $LaMnO_{3.13}$ (SG–CA) $LaMnO_{3.15}$ (SGP–PVA) and $La_{0.8}Sr_{0.2}MnO_{3.05}$ (SGP–PVA) are rhombohedral, $La_{0.9}Sr_{0.1}MnO_{3.01}$ (SGP–PVA) and $La_{0.9}Sr_{0.1}MnO_{3.07}$ (SG–CA) are cubic, whereas $LaMnO_{3.10}$ (SS) is orthorhombic and, finally, $La_{0.8}Sr_{0.2}MnO_{3.16}$ (SG–CA) is hexagonal. Note that there is an increase of the orthorhombic splitting for the treatment at 950°C in air. These conditions lead to a Mn^{4+} content of 20% in $LaMnO_{3.10}$ (SS). Lower calcination temperatures (600 and 700°C) yielded a slightly increased Mn^{4+} content (26%) and the rhombohedral phase was stabilized. On the other hand, $La_{0.9}Sr_{0.1}MnO_{3.07}$ is cubic for both calcination temperatures. This agrees with literature informations indicating that, at room temperature, a symmetry change from orthorhombic to rhombohedral occurs for Mn^{4+} concentrations >21% (i.e. $LaMn0_{3.105}$) [20]. The maximal Mn^{4+} content (52% in $La_{0.8}Sr_{0.2}MnO_{3.16}$) was obtained by applying the SG–CA preparation method. It exceeds the values obtainable by

usual high temperature synthesis as reported for $LaMnO_{3.12}$ (calcination in air at 1100–1200°C) [20]. Furthermore, it was reported that the distortion both of the unit cell and the MnO_6 octahedron, which is caused by replacing the Mn^{3+} by Mn^{4+}, may be partially recompensated by an equivalent substitution of La^{3+} cations by A^{2+} [13]. Therefore, with respect to the catalytic properties of the samples, the formation of various types of defect sites (cation vacancies or interstitial excess oxygen) has to be taken into consideration.

Concerning the formation of oxygen vacancies, various descriptions of the defect structure of $LaMnO_{3+\delta}$ were given in literature. The strontium substitution, taking place on the La^{3+} positions [22], was reported to effect the formation of oxygen vacancies [21]. Other sources concluded that the defect chemistry of $LaMnO_{3+\delta}$ is better described with randomly distributed La and Mn vacancies in equal amounts, rather than with oxygen excess interstitials [23]. Furthermore, a description of the defect structure of $LaMnO_{3.12}$ was given based on La and Mn vacancies with three times more La vacancies than for Mn [20].

The results presented here do not favor either one of the cited descriptions. At any rate, they show that the amount of Mn^{4+} increases with x=0.2. As mentioned above, the formation of oxygen vacancies as a result of cationic substitution occurs only if no Mn^{4+} is formed which is obviously not the case. It appears probable, therefore, that cation vacancies in the manganese sublattice present for x=0 were filled gradually by the strontium cations and at a certain x value the structure becomes oxygen-deficient. This means that both substitution phenomena are overlapping: filling of cation vacancies in the A sublattice without changes in the oxygen stoichiometry as well as substitution in the B sublattice without formation of B^{IV} but with changing oxygen content. This would qualitatively explain the trend of the TPIE data observed for low temperature oxygen uptake, as well as the trend of the catalytic activity (see below).

Oxygen exchange behavior

The aim of the ^{18}O isotope exchange experiments was to study the dependence of oxygen mobility on temperature and the Mn^{4+}/Mn^{3+} ratio both being related to the defect structure of the solid. The results of isotopic equilibration and exchange over $La_{1-x}Sr_xMnO_{3+\delta}$ presented in Figs 2 and 3 yielded the following statements.

For $LaMnO_{3.10}$ (SS), the s coefficient remains nearly constant proving that no oxygen uptake/release processes occur. For all other samples, between 152–300°C, the increasing s coefficient indicates that oxygen escapes from the solid. The $^{16}O_2$ content of the gas phase increases whereas the $^{18}O_2$ content (*m/e* not shown) decreases simultaneously. For the $La_{1-x}Sr_xMnO_{3+\delta}$ samples, this can be assigned to oxygen desorption accompanied by the reduction of Mn^{4+} to Mn^{3+}.

The complete heteromolecular oxygen exchange is the isotope exchange process occurring on all these samples $La_{1-x}Sr_xMnO_{3+\delta}$ under the measuring conditions. During ^{18}O isotope exchange measurements on $La_{1-x}Sr_xMnO_{3+\delta}$ considerable quantities of $^{16}O^{18}O$ were formed by homomolecular and partial heteromolecular exchange [5]. Moreover, traces of $^{16}O^{18}O$ were detected during the measurements, with a maximal

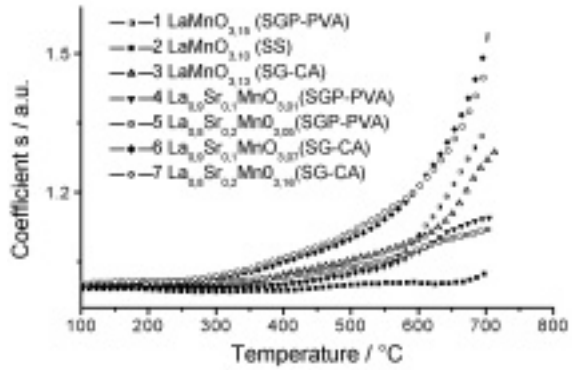

Fig. 2 Variation of the *s* coefficient indicating ^{16}O desorption from the solid

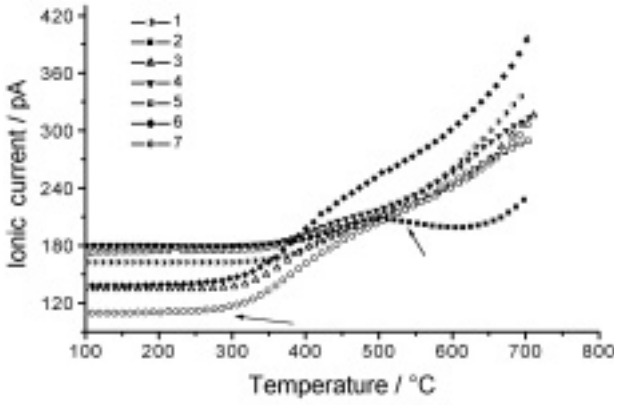

Fig. 3 IC curves for *m/e* 32 ($^{16}O_2$) for differently prepared $La_{1-x}Sr_xMnO_{3+\delta}$ (x=0, 0.1, 0.2) (For this and all further figures: numbers correspond to the substance formula as indicated in Fig. 2)

partial pressure of $^{16}O^{18}O$ at 650°C for $LaMnO_{3.10}$ (SS). The $^{16}O_2$ curve on $LaMnO_{3.10}$ (SS) exhibits a maximum at 500°C and a plateau between 500–510°C (Fig. 3), indicating hereby that homomolecular exchange is the predominant process. The starting temperatures of the partial heteromolecular exchange process are 417°C for $La_{0.8}Sr_{0.2}MnO_{3.16}$ (SG–CA), 429°C for $La_{0.9}Sr_{0.1}MnO_{3.07}$ (SG–CA), 440°C for $LaMnO_{3,15}$ and $LaMnO_{3,13}$, 450°C for $La_{0.8}Sr_{0.2}MnO_{3.05}$ (SGP–PVA), 460°C for $La_{0.9}Sr_{0.1}MnO_{3.01}$ (SGP–PVA) and 600°C for $LaMnO_{3,10}$ (SS). This means that $La_{0.8}Sr_{0.2}MnO_{3.16}$ (SG–CA) which has been prepared by the citrate method exhibited the highest ^{18}O exchange activity.

The interaction between $^{18}O_2$ and CH_4 under static conditions

The previously discussed changes in both the oxygen partial pressure and the isotope composition of the gas phase directly reflect the oxygen mobility in the solid. If a fur-

their reactant is present in the gas phase, e.g. CH_4 in our case, an attribution of isotope exchange phenomena to reactivity changes should be possible. Therefore, the methane oxidation with $^{18}O_2$ has been studied under the same conditions as described above, i.e. under static conditions. Figure 4 depicts the characteristic IC curve shape of the essential mass numbers allowing description of the interaction of a rather active catalyst, here $La_{0.8}Sr_{0.2}MnO_{3.16}$ (SG–CA), with gaseous $^{18}O_2$. The $^{16}O_2$ content in the gas phase increases due to complete heteromolecular ^{18}O exchange. The onset temperature for the $^{16}O_2$ release (180°C) is the lowest one for all investigated catalysts of this group. After the uptake of $^{18}O_2$ above 300°C, the CH_4 content decreases whereas CO_2 (*m/e* 44) and H_2O (*m/e* 18) appear. Summarizing these findings, it can be deduced that both the catalytic combustion of CH_4 and the oxygen isotope exchange occur via a complete heteromolecular mechanism. This means that the oxygen for the methane oxidation originates from the solid.

As the gas phase originally consists only of $^{18}O_2$, the absence of this isotope ^{18}O in the primary oxidation products (no formation of e.g. $C^{18}O_2$, $C^{16}O^{18}O$, $H_2{}^{18}O$ in significant amounts) clearly suggests that the oxidizing agent in the reaction is the metal in the high oxidation state, i.e. the oxygen liberated from the solid as a result of the change in oxidation state (Eqs 5–7).

$$CH_{4\,(g)}+4{}^{16}O^{2-}_{(s)} \rightarrow C^{16}O_{2\,(g)}+2H_2O_{\,(g)}+8e^- \quad (5)$$

$$8Mn^{4+}_{(s)}+8e^- \rightarrow 8Mn^{3+}_{(s)} \quad (6)$$

$$8Mn^{3+}_{(s)}+2{}^{18}O_{2\,(g)} \rightarrow 8Mn^{4+}_{(s)}+4{}^{18}O^{2-}_{(s)} \quad (7)$$

It should be noted that for prolongated reaction times, of course, the ^{18}O incorporation into the solid via the mentioned mechanism becomes more and more important. It begins with a very weak increase of the IC for *m/e* 46 ($C^{16}O^{18}O$, Fig. 4).

The lowest onset temperature for the methane oxidation (318°C) was detected in the case of $La_{0.8}Sr_{0.2}MnO_{3.16}$ (SG–CA) in Fig. 5. For the non-substituted $LaMnO_{3+\delta}$ samples,

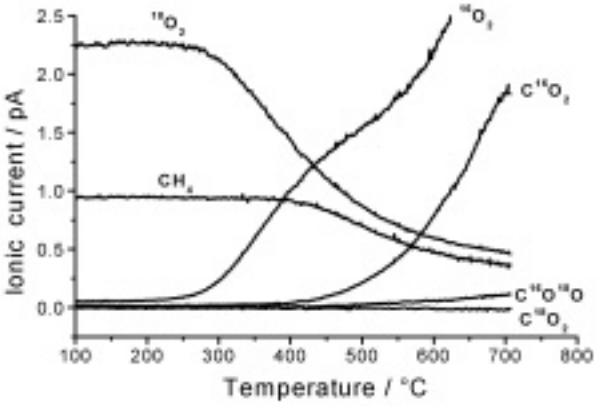

Fig. 4 IC curves for the essential species during CH_4 oxidation with $^{18}O_2$ on $La_{0.8}Sr_{0.2}MnO_{3.16}$ (educts – thin line)

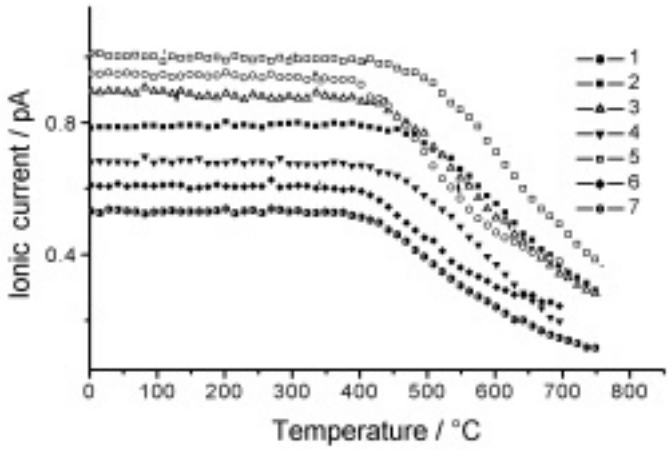

Fig. 5 IC curves for *m/e* 16 (CH_4) during CH_4 oxidation with $^{18}O_2$ on differently prepared $La_{1-x}Sr_xMnO_{3+\delta}$ (x=0, 0.1, 0.2)

the highest activity in both the ^{18}O exchange and oxidation reactions was found for the CA synthesis method. A comparison of the activity changes caused by the strontium substitution in the $La_{1-x}Sr_xMnO_{3+\delta}$ phases shows that the amount of oxygen liberated from the solid phase increases with increasing x. This means that the strontium replaced Mn^{III} thus increasing the Mn^{IV} content or decreasing the oxygen content.

It is noteworthy that phases with identical XRD pattern (e.g. the rhombohedral $LaMnO_{3.15}$ (SGP–PVA), $LaMnO_{3.13}$ (SG–CA), and $La_{0.9}Sr_{0.1}MnO_{3.05}$ (SGP–PVA) from Fig. 1) differ considerably in their capacity of oxygen sorption and, consequently, their isotopic exchange behavior.

The reaction between $^{16}O_2$ and CH_4 or CO in a flow reactor

The catalytic behaviour of $La_{1-x}Sr_xMnO_{3+\delta}$ ($0 \le x \le 0.2$) in both CO and CH_4 oxidation with normal oxygen $^{16}O_2$ under steady flow conditions is illustrated in Fig. 6. For temperatures between 25 and 150°C, the rate of carbon monoxide oxidation was highest over $La_{0.9}Sr_{0.1}MnO_{3.07}$ (SG–CA). For a degree of 50% CO conversion, the activity order is

$$La_{0.9}Sr_{0.1}MnO_{3.07}\ (SG–CA) > La_{0.8}Sr_{0.2}MnO_{3.16}\ (SG–CA) >$$

$$LaMnO_{3.13}\ (SG–CA) > LaMnO_{3.15}\ (SGP–PVA) > LaMnO_{3.10}\ (SS) =$$

$$La_{0.8}Sr_{0.2}MnO_{3.05}\ (SGP–PVA) > La_{0.9}Sr_{0.1}MnO_{3.01}\ (SGP–PVA).$$

The changes of the catalytic activity for the oxidative and related properties which were brought about by the Sr substitution of $LaMnO_{3+\delta}$ are compared in the same figure. Increasing x in the compounds $La_{1-x}Sr_xMnO_{3+\delta}$ leads to an increased oxygen release [24, 25]. In the present case, the maximum activity is achieved for 20% substitution of Sr for La. Indeed, oxygen vacancies are directly connected with the

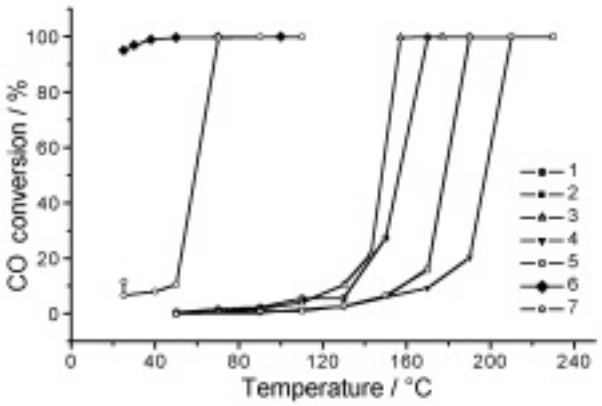

Fig. 6 Temperature dependence of the CO conversion for differently prepared $La_{1-x}Sr_xMnO_{3+}$ (x=0, 0.1, 0.2)

oxygen mobility. The higher the number of anion defects (the higher the value x), the higher is the oxygen mobility.

However, a too high oxygen release is accompanied by lowering the surface reoxidability [26], thus leading to a less active catalyst. This indicates that, as the x value increases, surface oxide ions tend to desorb, forming hereby coordinatively unsaturated B-site ions at the surface. The easier desorption of oxygen increases the oxidative power of the catalyst. These results totally confirm the conclusions of an earlier study [27] which stated that the controlling factor of the catalytic oxidation activity is (i) the oxidative power of the catalyst itself (expressed by the % CO conversion), (ii) the amount of oxygen which is easily adsorbed or desorbed and (iii) the capability of the surface for supporting the dissociation.

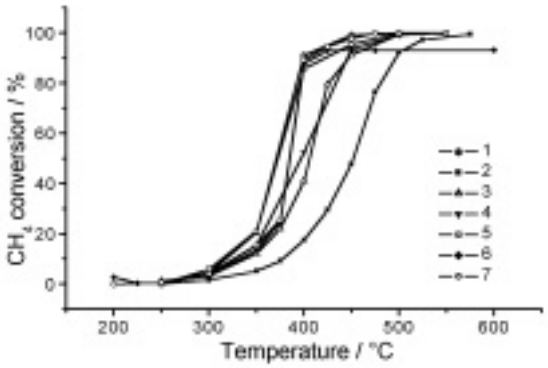

Fig. 7 Temperature dependence of the CH_4 conversion for differently prepared $La_{1-x}Sr_xMnO_{3+}$ (x=0, 0.1, 0.2)

Figure 7 depicts the CH_4 conversion upon oxidation. A differentiation of the catalytic activity in this series yields the following sequence of decreasing activity:

$LaMnO_{3.15}$ (SGP–PVA)>$La_{0.8}Sr_{0.2}MnO_{3.05}$ (SGP–PVA>

$La_{0.9}Sr_{0.1}MnO_{3.07}$ (SG–CA)=$La_{0.8}Sr_{0.2}MnO_{3.16}$ (SG–CA)>

$LaMnO_{3.13}$ (SG–CA)>$La_{0.9}Sr_{0.1}MnO_{3.01}$ (SGP–PVA)>$LaMnO_{3.10}$ (SS).

A comparison of Figs 6 and 7 shows that the CH_4 oxidation exhibits the differences in the conversion rates less than does the CO oxidation. A possible explanation is that higher temperatures are required for initiating the CH_4 oxidation and to maintain the reaction via a sufficient oxygen supply from the lattice. In the CO oxidation, on the other hand, the oxygen supply from the gas phase is considerable at temperatures which are too low for lattice oxygen diffusion within the catalyst.

Conclusions

It can be concluded that the predominant reaction occuring during the interaction of gaseous oxygen with $La_{1-x}Sr_xMnO_{3+\delta}$ phases of different preparation is not the reaction with dioxygen from the gas but with the nucleophilic oxide ions from the solid. The oxygen release is a consequence of the change in oxidation state of the manganese which can be influenced by cationic substitution taking place both in the lanthanum and/or the manganese sublattices.

Sol–gel related preparation routes that differ from the usual high-temperature synthesis allow the formation of crystalline perovskites as well. Both the higher Mn^{IV} content and, to a certain extent, the enlarged surface contribute to the higher catalytic activity of the $La_{1-x}Sr_xMnO_{3+\delta}$ phases.

References

1 M. Maciejewski, C. A. Müller, R. Tschan, W.-D. Emmerich and A. Baiker, Thermochim. Acta, 295 (1997) 167.
2 M. Mittleman, Thermochim. Acta, 166 (1990) 301.
3 D. Martin and D. Duprez, J. Phys. Chem., 100 (1996) 9424.
4 E. Kemnitz, A. A. Galkin, T. Olesch, S. Scheurell, A. P. Mozhaev and G. N. Mazo, J. Thermal Anal., 48 (1997) 997.
5 I. A. Koudriashov, G. N. Mazo, I. K. Murwani, S. Scheurell and E. Kemnitz, J. Therm. Anal. Cal., 63 (2001) 59.
6 A. Lindstedt, D. Strömberg and M. A. Milh, Appl. Catal. A116 (1994) 109.
7 N. Mizuno, M. Tanaka, and M. Misono, J. Chem. Soc. Faraday Trans., 88 (1992) 91.
8 N. M. Sammes and B. L. Kennedy, J. Mat. Sci. Lett., 15 (1996) 1839.
9 A. K. Ladavos and P. J. Pomonis, J. Chem. Soc. Faraday Trans., 87 (1991) 3291.
10 P. Salomonsson, Appl. Catal. A104 (1993) 175.
11 K. S. Chan, J. Ma, S. Jaenicke and G. K. Chuah., Appl. Catal., A 107 (1994) 201.
12 N. M. L. N. Closset, R. H. E. Van Doorn and H. Kruidhof, Powder Diffr., 11 (1996) 31.
13 J. A. Alonso, M. J. Martinez-Lopez and M. T. Casais, Eur. J. Sol. State Inorg.Chem., 33 (1996) 331.

14 C. Vázques-Vázques, M. C. Blanco, M. A. López-Quintela, R. D. Sánches, J. Rivas and S. B. Oseroff, J. Mater. Chem., 8 (1998) 991.
15 E. Kemnitz, D.-H. Menz, C. Stöcker and T. Olesch, Thermochim. Acta, 225 (1993) 119.
16 V. S. Muzikantov, V. V. Popovski and G. K. Boreskov, Kin. i Katal., 5 (1964) 624.
17 G. K. Boreskov, Adv. Catal., 15 (1964) 285.
18 V. S. Muzikantov, G. I. Panov and G. K. Boreskov, Kin. i Katal., 14 (1973) 948.
19 Yenxing Ye, Longtu Li, Ji Zhou, Hungguo Zhang and Zhilun Gui, Mater. Sci. Eng., B64 (1999) 68.
20 B. C. Tofield and W. R. Scott, J. Solid State Chem., 10 (1974) 183.
21 S. T. Aruna, M. Muthuraman and K. C. Patil, J. Mater. Chem., 7 (1997) 2499.
22 J. A. Alonso, M. J. Martinez-Lopez, M. T. Casais, J.-L. MacManus-Driscoll, P. S. I. P. N. de Silva, L. F. Cohen and M. T. Fernandez-Diaz, J. Mater. Chem., 7 (1997) 2139.
23 J. A. M. van Roosmalen, E. H. P. Cordfunke, R. B. Helmholdt and H. W. Zandbergen, J. Solid State Chem., 110 (1994) 100.
24 L. Marchetti and L. Forni, Appl. Catal.: B Environmental, 15 (1998) 179.
25 K. Tabata, I. Matsumoto and S. Kohiki, J. Mater. Sci., 22 (1987) 1882.
26 N. Yamazoe and Y. Teraoka, Catalysis Today, 8 (1990) 175.
27 T. Nitadori, S. Kurihara and M. Misono, J. Catal., 98 (1986) 221.